Materials Today Communications 36 (2023) 106802

Contents lists available at ScienceDirect

Materials Today Communications

journal homepage: www.elsevier.com/locate/mtcomm

Dry reforming of methane with CO_2 over Co-$La_{1-x}Ca_xNiO_3$ perovskite-type oxides supported on ZrO_2

Babalola Aisosa Oni [a,*], Olusegun Stanley Tomomewo [a], Samuel Eshorame Sanni [b,*], Victor Oyebamiji Ojo [c]

[a] Department of Energy Engineering, University of North Dakota, Grand Forks, 58203, North Dakota, United States
[b] Department of Chemical Engineering, Covenant University, Km 10 Idiroko road, Ota, Nigeria
[c] Department of Mechanical Engineering, University of North Dakota, Grand Forks, 58203, North Dakota, United States

ARTICLE INFO

Keywords:
CO_2
Perovskite-type oxides
Co catalyst
CH_4 dry reforming
Carbon deposition, Nickel

ABSTRACT

Under methane dry reforming conditions, Co has an impact on the stability and activity of Co-$La_{1-x}Ca_xNiO_3$-ZrO_2 catalyst. In the course of the reduction reactions of perovskite precursors, the catalytic performance of Co-based bimetallic catalyst was evaluated. TEM, BET, H_2-TPR, TGA, NH_3-TPD, XRD and CO_2-TPD techniques were used to characterize the catalyst and investigate the metal-metal/metal-support interactions as well as the phase changes that occurred under the reaction conditions. The catalyst with the highest activity was the 2%Co- $La_{0.2}Ca_{0.8}NiO_3$-ZrO_2 due to the synergistic interaction between Ni (in the perovskite) and Co. Thus, the inclusion of Co in the catalyst, promoted the removal of carbonaceous deposits from its surrounding active sites, which in turn improved the catalyst's activity and stability. The synergistic effects of Ni-Co in the catalyst's lattice, enhanced the catalyst's performance as well as reduced the formation of carbon. Therefore, the 2%Co-$La_{0.2}Ca_{0.8}NiO_3$-ZrO_2 exhibited the most excellent catalyst stability, activity and the mildest carbon deposition with high CO_2 and CH_4 conversions of 90% and 88% respectively.

1. Introduction

The world's global energy demand is progressively growing and is currently mounting so much pressure on the depletion of conventional fossil fuels, hence the drift towards the exploration/exploitation of new energy sources all aimed at ensuring a low-carbon economy [1]. Meanwhile, since CO_2 is one of the primary greenhouse gases (GHGs) and a common waste gas in the chemical and energy sectors, its direct use is a sure way to reduce carbon emissions [2,3]. Furthermore, there have lots of investigations into the novel use of CO_2 as a result of its increased threats posed by climate change [4]. One of such new approaches is the reaction of CH_4 and CO_2 to produce syngas; carbon dioxide reforming of methane (dry reforming) offers a suitable solution to these major issues that confront the modern society [2,3]. As a result, the effective use of methane, alongside low carbon recycling in the framework of carbon capture, utilization and storage the dry reforming of methane (DRM) via CO_2 to produce synthesis gas has become more appealing [5,6]. In DRM, two significant GHGs are transformed into syngas as presented in (1).

$$CO_2 + CH_4 \rightarrow 2CO + 2H_2 \quad (1)$$

Fischer Tropsch (F-T) synthesis is a process in which hydrocarbon is synthesized from syngas under suitable conditions. This gas serves as a bridge between a variety of useful fuels, chemicals and longer-chain hydrocarbons [3]. Depending on the catalyst used, an H_2/CO ratio of around 1 is needed for the efficient downstream processing of the reformed gas into synthesis gas [7]. The H_2/CO of the resulting synthesis gas obtained from the DRM process is close to 1 and may therefore be easily employed in the F-T synthesis of liquid hydrocarbons [8]. Syngas can be obtained from the steam reforming reaction of methane above 800 °C, however, the resulting stoichiometric H_2/CO ratio of 3 under such condition is undesirable for the downstream processing of the product-gas.

Several works involving the use of different catalysts in the dry reforming of methane have been reported [4,6–8]. However, due to the strong propensity for coking and catalyst-deactivation to set in when these catalysts are employed, their continuous use is currently being discouraged. Undesirable H_2/CO ratios may ensue as a result of side reactions imposed by the Boudouard reaction ($2CO \leftrightarrow CO_2 + C$) alongside CH_4 cracking, and the RWGS reaction, which subsequently

* Corresponding authors.
E-mail addresses: oni.babalola@und.edu (B.A. Oni), samuel.sanni@covenantuniversity.edu.ng (S.E. Sanni).

https://doi.org/10.1016/j.mtcomm.2023.106802
Received 29 May 2023; Received in revised form 23 July 2023; Accepted 1 August 2023
Available online 2 August 2023

Nomenclature

DRM	Dry methane reforming
GHG	Greenhouse gases
RWGS	Reverse water-gas shift reaction

cause carbon and water to be deposited and produced respectively [9,10].

For DRM reaction, transition metals like Pt, Ru, Ni, Rh, Pd, Ir and Co are frequently regarded as the most prominent catalysts [11]. Noble metals like Ru, Rh or Pt may not likely to form coke, however, they are very expensive and costly and are not economically viable [3,7]. Co and Ni are thus perhaps the most desirable DRM catalysts from an economic standpoint, since they combine high dry methane reforming activity with a relatively low cost [11]. Furthermore, Ni exhibits high rate of coke production and sintering, which are two significant drawbacks associated with the use of the catalyst. Literature also has it that coke production at high temperatures is primarily caused by methane breakdown ($CH_4 \rightarrow C + 2H_2$) [12].

ABO_3 is the general chemical formula for perovskites i.e., metal oxides containing two metal cations. These perovskites are employed for DRM reactions. The metal "B" provides the active site, while the metal "A" stabilizes and improves catalysis [8]. Substituting B or A ions with hetero-valent metal ions can modify the catalyst's structure, thus creating O_2 vacancies or valence states of the original metal cation, which in turn improves the overall redox characteristics and O_2 mobility. La oxides help to homogeneously disperse Ni; thus Ni-catalyzed DRM reactions are more stable with La. La increases the catalyst surface area, Ni buildup as well as the medium's basicity [13]. By increasing the number of NiO sites, there is an increase in the reforming reaction and reduced carbon deposit by promoting Ni species' reducibility and carbon gasification. The $LaNiO_3$ catalyst for methane steam and CO_2 reforming is well distributed and resistant to coke deposition [14]. La supported Ni catalyst reduces the abundance of Ni, improves, as well as stabilizes, and restricts water gas shift (RWGS) reaction.

Thermal effect, alongside acid-base and reduction-oxidation capabilities of each component that make up the oxide, provide ZrO_2 with a better active metal support than either of its components as well as its other counterparts. When used as DRM support, ZrO_2 supported on Ni catalysts will benefit from the material's outstanding redox characteristics by preventing the development of carbonaceous deposits thus increasing the catalyst's lifetime [15].

Oxygen storage and lattice oxygen mobility also increase catalyst activity in co-substituted perovskites. The Co creates oxygen vacancies, which activates oxygen species to expel carbon from the catalyst [16]. Ca improves catalytic activity by dispersing surface-active components, whereas the strong bond that exists between Ni and Co helps to prevent crystal formation. The dispersion of Ni has also been observed to reduce the size of Ni [17]. Due to its chemical and thermal characteristics, Ca promotes or supports catalyst activity. In addition, nano-catalysts benefit from the thermal stability exhibited by Zr in addition to its redox chemistry, and oxygen-transporting capacity.

Since various researchers have suggested that the Ni-Co alloy has a good thermal stability and coke resistance, it then implies that the Ni-Co combination is of special relevance in this regard [18]. For instance, bimetallic catalysts such as those of Ni-Co combinations, have been found to exhibit increased catalyst performance in processes such as dry reforming reactions of methane [8], CH_4 partial oxidation [10,13] and biomass steam reforming reactions [12]. According to Wang et al. [19], the lattice configuration in the alloying of Co and Ni on atomic level, makes the contact between Nickel and Cobalt stronger than what exists between Nickel and other oxides. Kumar et al. [20], demonstrated that Ni and Co interaction promoted metal particle dispersion and thus induced smaller Nickel particles, which increased coke resistance and catalyst activity. According to the authors, the high metal dispersion of the Ni-Co catalyst is what accounts for its exceptional performance [21]. In the partial oxidation of methane, Yentekakis et al. [22] found that Ni-Co/$CaAl_2O_4$/A_2O_3 catalysts performed more efficiently compared to those bearing mono-metallic Co catalysts. San José -Alonso et al. [23] produced Ni-Co/Al_2O_3 catalysts and concluded that the catalysts with the highest contents of Co were most active, because their results exceeded the methane conversion of Ni-Al_2O_3 by approximately 18% after 5 h of reaction. Also, literature has it that, the incorporation of Co as support for Perovskite type oxide catalysts can produce an improved synergistic effect, which changes the catalyst's features including its nature, structure, metal-support interaction, and particle size [26].

The use of a bimetallic Ni-base Perovskite type oxide-Co catalyst supported on ZrO_2 during dry reforming of methane has never been studied in terms of the synergetic effects imposed by the metal species on the catalyst's properties, especially in terms of its performance as imposed by its mesoporous structure, which may require further insight. According to ref. [27], perovskites provide the oxygen species needed to react with the carbon that has been deposited on the Co crystallites and thus restore the active sites/surface of the catalyst. Additionally, a variety of metal cations can be included in the perovskite matrix [28]. $La_{1-x}Sr_xNi_{1-y}Co_yO_3$ [29], $LaNi_{1-x}Co_xO_3$ [30] and $La_{2-2x}Sr_{2x}NiO_4$ [31] have been reported as catalyst precursors tried in dry reforming reactions of methane. Because the ionic radius of Co^{3+} is similar to those of the Ni^{3+} sites in perovskites, Ni can be easily replaced with Co [32]. Thus, the Ni- base perovskite type oxide-Co catalyst supported on ZrO_2 is believed to have suppressed the carbon deposition by stimulating the activation of CO_2 [6,33] on the catalyst's surface.

Therefore, this study focuses on the use of Ni- base perovskite type oxide-Co catalysts supported on ZrO_2 that will optimally suppress the carbon deposition. The choice of the catalyst adopted was decided based on its activity, stability and mild carbon deposition with high CO_2 and CH_4 conversion due to the synergistic interaction between Ni (in the perovskite) and Co. Thus, the inclusion of Co in the catalyst promotes the removal of carbonaceous deposits from the surrounding active sites, which in turn increases the catalyst's activity and produces a catalyst with improved stability.

In order to overcome the deactivation issue of the catalyst for carbon dioxide reforming of CH_4, this study employs a novel strategy that combines various catalytic features to enhance the performance and stability of the catalyst in a single system. The sintering effect of Ni was intended to be eliminated or inhibited in the developed catalyst described in this work by increasing the catalyst's thermal stability with the help of perovskites of high melting points. The desired surface area for high catalyst activity seen to be inherent in ZrO_2 owing to its characteristic high surface area.

2. Materials and method

2.1. Preparation of the catalysts

The co-precipitation method was used to prepare the desired catalyst. The preparation involves the use of zirconia nitrate (J.T Baker) and $Co(NO_3)_2{\cdot}6\ H_2O$ (Sigma Andrich Co., Ltd.) as precursors, which were dissolved in de-ionized water. The resulting solution was further co-precipitated using aqueous caustic soda solution within a pH ranging from 9 to 10 and concentration of 1 mol/L. The slurry obtained was then aged and agitated for 3 h at 28 °C before being washed with deionized water for 24 h. The supernatant solution was filtered off; the precipitate was oven dried at 105 °C and thereafter, calcined for 4 h at 800 °C. In order to evaluate the synergetic interactions between the cobalt and Zr catalysts, a precursor ratio of 1:1 was maintained for $Co(NO_3)_2{\cdot}6\ H_2O$ and $Zr(NO_3)_4$.

2.2. Synthesis of perovskite-type oxides

Perovskite-type oxide $La_{1-x}Ca_xNiO_3$ with different electronic configurations (x = 0, 0.2, 0.4, 0.6 and 0.8) were synthesized using a modified citrate technique [31]. A concentrated citric acid solution (Sigma Aldrich) was prepared and added to a precursor-solution of the B-site cation $Ni(NO_3)_2{\cdot}6\ H_2O$ with an excess of ethylene glycol and stirred for 1 h at 60 °C with a magnetic stirrer. Calcium nitrates and lanthanum solutions were added to the mixture and the mixture was continuously stirred for 1 h at 60 °C. The obtained solution was evaporated slowly at 105 °C for 24 h until a spongy substance was produced. To produce the finished mixed oxide, the citrate precursor was crushed, decomposed at 600 °C for 2.5 h, and then calcined at 850 °C for 11 h. The ratio of the mixture of Co: ZrO_2:$La1_{-x}Ca_xNiO_3$ is 1:1:1. Finally, the Co/ZrO_2 hybrid was mixed with $La_{1-x}Ca_xNiO_3$ in different electronic configurations (x = 0, 0.2, 0.4, 0.6 and 0.8); the molar/weight ratio of Ni and Zr in the catalyst used in carrying out this work is 1:1.

2.3. Characterization techniques

Transmission electron microscopy (TEM), Thermogravimetric analysis, temperature-programmed oxidation and reduction, BET surface area, and X-ray diffraction (XRD), were used to characterize the different samples. The Brunauer-Emmett-Teller (BET) specific surface areas were calculated using nitrogen physisorption isotherms at − 196 °C (Tristar-micrometric equipment, XLT-300). The Cu Kα_1(λ = 1.54Å) radiation at 40 mA and 45.0 kV, XRD patterns were captured on a Philips diffraction system. Images of the TEM were captured using a Philips CM-2000 microscope operating at 200.0 kV. An Automatic Chem II 2900 computer with a TCD conductor was used to perform the H_2-TPR (TCD). 50 mg of the catalyst was heated to 150 °C (at an interval of 10 °C/min) under Ar (Core-gas Ar, > 99.9%) for 30 min before being cooled to 40 °C at a temperature reduction rate of 5 °C/min. The samples were heated to temperatures between 50 and 850 °C at a rate of 10 °C/min while being infused with 5 vol% H_2 in Ar at a volumetric flow rate of 50 mL/min. TPD- NH_3/ CO_2, was used to study the basicity and acidity of the catalyst. 50 mg of the material was analyzed using the Automatic Chem II 2900 machine. The catalysts were pre-treated for 30 min at 200 °C (5 °C/min) under Helium (Coregas, > 99.9%), and then cooled to 40 °C (at 5 °C/min). The samples were further saturated for an hour at 20 mL/min with Core-gas, 5.1% ammonia, ammonia-helium or Core-gas carbon dioxide, 1% carbon dioxide nitrogen. By flushing the catalyst with helium for one hour and then heating it from 40° to 800°C at 10 °C/min, physisorbed molecules were eliminated. Using a Micromeritic-3000 device, the mesoporous structure and catalysts' surface areas were evaluated using the BET method (nitrogen gas adsorption). The samples were degassed at 190 °C before the test. The investigation of the desorption profile of the isotherm was used to determine the pore size distributions of the materials using the Barrett-Joyner-Halender (BJH) model. The Thermo Fisher Scientific 255 X-1 analyzer was used to analyze the X-ray photoelectron spectra (XPS) at 28 °C (room temperature) with

a Mg-anode under Kα ($h\nu$ = 1487.3 eV) radiation.

2.4. Dry reforming of methane

The CH_4-carbon dioxide reforming reaction was conducted in a quartz tube fixed-bed reactor (300 mm long, ID, 6.0 mm) using 0.1 g of catalyst (0.25 mm) mixed with quartz sand weighing 0.3 g. The desired compositions of reactant gases were fed through a mass-flow controller having a gas hourly space velocity (GHSV) of 32 L $g^{-1}h^{-1}$ in a ratio of 1:1:1 (methane: nitrogen gas: carbon dioxide). Before the commencement of reaction, the catalysts were heated for 2 h at 800 °C (10 °C/min) under a 25% hydrogen/nitrogen gas atmosphere (80 mL/min) for 2.5 h. After heating, nitrogen gas (> 99.99%) was used to purge the reactor for 10 min before the feed was charged to the reactant gases. The methane and carbon dioxide purity used for the experiment were > 99.95% and > 99.99% respectively. All gases were supplied by BOC gas limited, Oshodi, Lagos, Nigeria. With the quartz sand and catalyst mixture in the center of the reactor, analysis was conducted at 800 °C. Product gases were examined using an online gas chromatograph (GC) fitted with a TDX-010 column alongside a TCD detector. A cold trap was positioned before the TCD so as to eliminate any traces of water present in the gases. Without catalyst charge, a blank test revealed that the CH_4 conversion at 800 °C was less than 5%. Eqs. 1 and 2 present the calculations for converting carbon dioxide or methane into a fraction or percentage of each feed.

$$X_{CH_4}(\%) = \left(\frac{F_{CH_4,in} - F_{CH_4,out}}{F_{CH_4,in}}\right) \times 100 \quad (1)$$

$$X_{CO_2}(\%) = \left(\frac{F_{CO_2,in} - F_{CO_2,out}}{F_{CO_2,in}}\right) \times 100 \quad (2)$$

where F_{CH_4,CO_2}, out represents the molar flow rate of the component CH_4/CO_2 in the out gas and F_{CH_4,CO_2}, in is the molar flow rate of CH_4/CO_2 in the feedstock.

3. Results and discussion

3.1. Textual and structural properties of the catalyst

Table 1 presents the optimum textural properties of all the synthesized catalysts. It can be observed that the relative content of Co and La was changed at the same time. The change of La-Ca content has a certain impact on the structure and activity of the catalysts. Co has an impact on the stability and activity thus promoting the removal of carbonaceous deposits from the surrounding active sites, which in turn increases the catalyst's activity and produces a catalyst with improved stability. According to Fig. 1, the nitrogen gas adsorption-desorption isotherms for all the analyzed catalysts are typical of mesoporous, highly structured and microporous materials (Type IV). Depending on the series, the Ni-Co loaded catalysts have high surface areas, above 80 m^2/g. Thus, 2% Co-$La_{0.2}Ca_{0.8}NiO_3$- ZrO_2 displayed the highest surface area of 159 m^2/g due to the presence of large Ca and lower La oxide in the perovskite catalyst, as well as the %Co loading which influences the textural and structural properties of the Co-loaded catalysts since it has the capacity to limit/prevent carbon deposits relative to other catalysts. Al-Fatesh et al., [1] and Zhu et al. [2] stated that a catalyst's activity promoted with CaO displayed a high affinity for chemisorption of carbon dioxide which enhanced the catalyst's thermal stability and in turn reduced its propensity for coke deposition. Adsorption capacity and thermal stability are both important characteristics of microporous materials which are used as adsorbents and promoters for catalysts. The %Co loading on the

Table 1
The different catalyst configurations adopted during CO_2 reforming of CH_4.

Parameter (Series)	Catalyst optimum performance	BET surface area (m^2/g)	Average pore width (nm)	Pore volume (cm^3/g)
$x = 0.0$	0.5% Co-$La_1Ca_0NiO_3$- ZrO_2	82	0.82	2.89
$x = 0.2$	1.5% Co-$La_{0.8}Ca_{0.2}NiO_3$-ZrO_2	94	0.76	2.82
$x = 0.4$	2%Co-$La_{0.6}Ca_{0.4}NiO_3$-ZrO_2	99	0.88	3.00
$x = 0.6$	1.5%Co-$La_{0.4}Ca_{0.6}NiO_3$-ZrO_2	107	0.69	2.79
$x = 0.8$	2% Co-$La_{0.2}Ca_{0.8}NiO_3$-ZrO_2	159	0.52	2.37

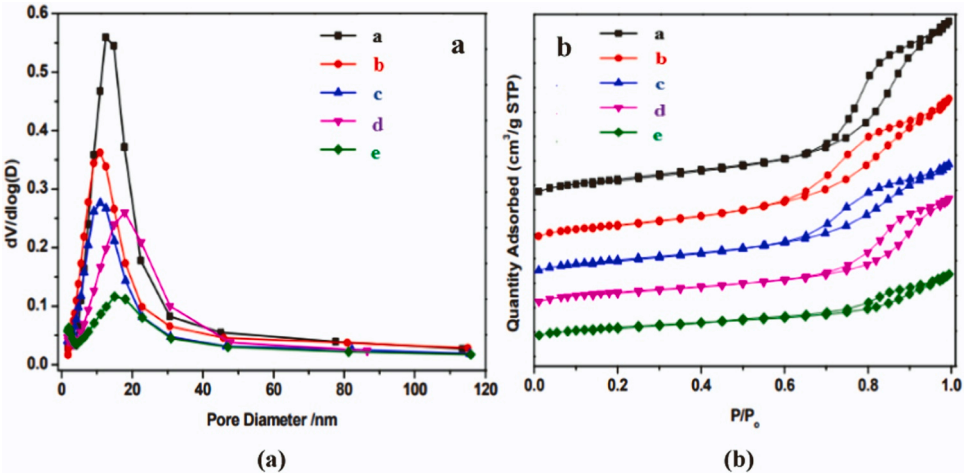

Fig. 1. N_2 adsorption-desorption isotherms with varying (a) dv/dlog(D) vs pore diameter (b) volume of N_2 gas adsorbed vs relative pressure (equilibrium pressure/ saturation pressure= P/Po) (a) 2% Co- $La_{0.2}Ca_{0.8}NiO_3$- ZrO_2; (b) 1.5%Co- $La_{0.4}Ca_{0.6}NiO_3$- ZrO_2; (c) 2%Co- $La_{0.6}Ca_{0.4}NiO_3$- ZrO_2 (d) 1.5% Co- $La_{0.8}Ca_{0.2}NiO_3$- ZrO_2; (e) 0.5% Co- $La_1Ca_0NiO_3$- ZrO_2.

Perovskite-type oxides supported on ZrO_2, greatly influenced the surface area of the catalyst. According to San José -Alonso et al. [23], although a Co rich catalyst may perform well during dry reforming of methane, it needs to be modified to prevent the deposition of carbon. Furthermore, Han et al. [34] observed that the strong metal-support contacts, greatly dispersed the active metal as well as improved the synergetic effects offered by the Ni-Co bimetallic catalyst, which resulted in a high tendency for coke formation. These findings show that the grafting of nickel and cobalt species into the bimetallic Ni-Co catalyst framework, occurred synergistically; consequently, different Ni/Co proportions can significantly affect the catalysts physicochemical properties, which may alter the performance of the catalyst alongside its coking behavior during the DRM reaction.

Fig. 1 displays the N_2 adsorption-desorption isotherms and pore size distribution of the catalysts. According to the IUPAC guidelines, catalysts of this type are of type IV isotherms, which shows that the samples' architecture included mesoporous frameworks with simple pore connectivity. The mesoporous framework is highly efficient in preventing the sintering of Ni-Co at elevated temperatures as reported by Guo et al. [28]. In addition, as a result of the catalyst's high surface area, it is expected that the 2%Co-$La_{0.2}Ca_{0.8}NiO_3$-ZrO_2 interface was highest, which is crucial for high catalyst performance. The change in the La-Ca content has a certain impact on the structure and activity of the catalysts, which is evident in the dry reforming of methane with CO_2.

It is interesting to note that all of the analyzed catalysts were prepared under the same conditions [29]. It was also reported that the catalysts were seen to possess slit-like pores that were formed as a result of the buildup of aggregated particles [28]. These findings suggest that the difference between Ni and Co species during catalyst preparation influences the development of the final catalysts' porous structures, which may be related to the initial characteristics of the particles or ions (e.g. crystal size, ionic charges, spatial orientations, ionic diameters etc.). The pore size distribution of the catalyst was calculated using the BJH method. All the Ni-Co catalysts exhibited significantly developed porous structures as seen in Fig. 1a. In addition, the pore diameters of the 2%Co-$La_{0.6}Ca_{0.4}NiO_3$-ZrO_2 material revealed a broader distribution with a preference for smaller pores due to the synergistic interactions between Ni and Co.

Note: Pls find out the meanings of P/Po and the differential term at the ordinate of Fig. 1a and include them in the caption of Fig. 1a.

3.2. X-ray diffraction

There were hardly any additional phase-impurities in the perovskite powder samples, which appeared typically crystalline (Fig. 2). For all the perovskite catalysts, there were primarily five distinctive diffraction peaks of Ni-Co at $2\theta = 31.19°$, 37.01°, 45.07°, 60.48°, and 66.03°, which correspond to the crystal planes (2 0 0), (3 1 1), (4 0 0), (4 4 0) and (5 1 1) respectively. All of the patterns for the catalysts showed broad diffraction peaks, which are reflective of well-defined nanocrystalline frameworks. A highly broad diffraction peak at $2\theta = 36.19^o$ which corresponds to NiO, was found in the 1.5%Co-$La_{0.4}Ca_{0.6}NiO_3$-ZrO_2 and 1.5%Co- $La_{0.8}Ca_{0.2}NiO_3$-ZrO_2 catalysts, whereas the low-intensity diffraction peaks centered at $2\theta = 32.19^o$ and 65.3 ^{o} in the Co-rich samples were attributed to the presence of Co_3O_4. Despite its formation at high calcination-temperature, the Ni-Co spinel phase in the 2% Co-$La_{0.6}Ca_{0.4}NiO_3$-ZrO_2 was not observed in the diffractions received for the Ni-Co pairs [21,30]. These attributes were also mentioned by Luisetto et al. [31], wherein it was observed that the catalyst's strong metal-support interaction (SMSI) constrained the potential for Ni^{2+} and Co^{3+} species to bond together. Due to high dispersion of CoO and NiO, brought on by the SMSI effect, no signal of NiO or CoO appeared in the diffraction patterns of the 2%Co- $La_{0.6}Ca_{0.4}NiO_3$-ZrO_2 sample. The ZrO_2 support maintained a typical amorphous form, which reveals the occurrence of mesoporous and microporous frameworks after the treatment of the catalysts. The related crystal phases of La were observed which makes for its uniform dispersion in the catalyst.

3.3. Effect of particle size distribution of catalysts for DRM

The microstructures of the prepared catalysts were further explored

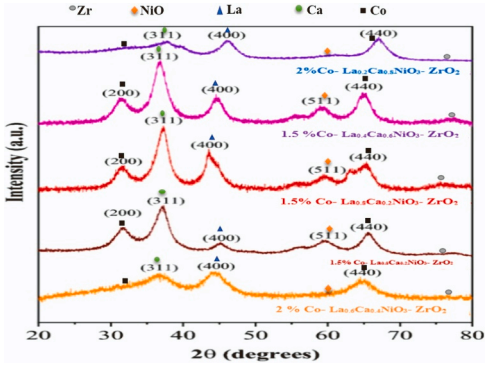

Fig. 2. The XRD patterns of the intensity of light on the Co- $La_{1-x}Ca_x$-NiO_3.ZrO_2 catalysts.

by TEM. The presence of the Ni-Co species was established by TEM (Fig. 3 a2-e3). The TEM characterization results further proved that all the analyzed samples appeared like nano-sheets, and that the catalysts were uniformly dispersed in the substrate (Fig. 3(a2–e3)). The histogram (Fig. 3a1-e1) shows the size distribution of various catalysts. The average particle sizes of all catalysts were measured using TEM and the results obtained suggest that Fig. 3 (a1-a3): (2%Co- $La_{0.6}Ca_{0.4}NiO_3$- ZrO_2) is 5.3 nm, Fig. 3 (b1-b3):(0.5% Co- $La_1Ca_0NiO_3$- ZrO_2) is 4.8 nm, Fig. 3 (c1-c3): (1.5% Co- $La_{0.8}Ca_{0.2}NiO_3$- ZrO_2) is 9.4 nm, Fig. 3 (d1-d3): (1.5%Co- $La_{0.4}Ca_{0.6}NiO_3$- ZrO_2) is 9.5 nm and Fig. 3 (e1-e3): (2% Co- $La_{0.2}Ca_{0.8}NiO_3$- ZrO_2) is sized 10 nm, respectively. This is in line with the particle size distribution result of Co- $La_{1-x}Ca_xNiO_3$.ZrO_2 as determined from the XRD (Fig. 2). Fig. 3 demonstrates the presence of embedded Ni and Co nanoparticles in the Co- $La_{1-x}Ca_xNiO_3$.ZrO_2. Because of its distinctive mosaic design, which effectively prevents Ni nanoparticle migration and aggregation, the catalyst is more stable. Even so, there was barely any overlap between the Ni nanoparticles of different diameters during the reaction.

3.4. H_2-TPR analysis

H_2-TPR investigates the reducibility of the catalyst. The H_2-TPR of the catalysts for CO_2 DRM is presented in Fig. 4. The two reduction peaks show how the presence of ZrO_2 influenced the H_2-TPR profile of the catalysts. The first peak is ascribed to oxygen adsorption onto the surface defects of Ni-Co at low temperatures, and the second peak can be attributed to the development of Ni^{2+} and Co^{3+} in the bulk phase of the catalyst at approximately 600 °C. Three peaks are shown in the H_2-TPR profiles for the Co- $La_{1-x}Ca_xNiO_3$.ZrO_2 samples, which indicate the reduction of three different forms of reducible metal oxide species, known as α, β and γ from low to high temperature. The surface oxygen found in the Co surface defects, was attributed to the low intensity peak "α" that was visible at low temperatures (i.e., within 170–360 °C). The NiO species that had weak interactions with Co corresponded to the peaks observed at about 400 °C. The reduced NiO, which significantly interacted with the Co substrate in the mixed spinel-phase of Co- $La_{1-x}Ca_xNiO_3$.ZrO_2, generated the peak, which occurred at about 500 °C [32,33]. The reduction of nickel and cobalt in the highly complex, spinel-like quaternary phase is likely the reason for the reduction peaks seen in the Ni-Co catalyst at near 400 and 500 °C. It was observed that the increased interactions between NiO and Co-produced by the increase in %Ni, caused the peak to shift towards higher temperatures. This informs that catalysts with higher Ni percentages had higher concentration of metallic Ni. As a result of the higher volume of H_2 required for the reduction of the catalysts with higher Ni contents, the area of the reduction peaks in the TPR profiles of the catalysts with higher percentage of Ni were larger than the areas detected for the catalysts with lower percentages of Ni [35]. The Ni-Co catalyst's maximum peak-reduction occurred at 850 °C. The occurrence of nickel and cobalt atoms on the surface of the catalyst are more easily accessible than those in the bulk structures; this can be attributed to the surface enrichment of nickel and cobalt in the Ni-Co catalyst. The catalyst with the highest La_2O_3 loading catalyst gave the highest peak-shift. This means that the addition of La_2O_3 helped to further increase the interaction between the NiO and the modified support. Table 2 presents the quantitative analysis of the degree of reduction of nickel catalyst (active phase) during H_2-TPR.

3.5. NH_3-TPD

The NH_3-TPD profile of acid properties of the catalysts are presented in Fig. 4. In order to facilitate ammonia adsorption and activation at the active sites of the catalysts during the reaction steps, a suitable NH_3- TPD catalyst should have the required number of acid sites [35–37]. At 100–200 ∘C, the observed peak suggests the presence of weak acid-sites [32]. The degree of acidity of the 2% Co- $La_{0.2}Ca_{0.8}NiO_3$- ZrO_2 is considerably higher than those of 1.5%Co- $La_{0.4}Ca_{0.6}NiO_3$- ZrO_2, 1.5% Co- $La_{0.8}Ca_{0.2}NiO_3$- ZrO_2, 2%Co- $La_{0.6}Ca_{0.4}NiO_3$- ZrO_2 and 0.5% Co- $La_1Ca_0NiO_3$- ZrO_2 respectively. Three peaks were observed at 145, 383 and 452 °C in the Perovskite-type oxides, due to the NH_3 desorbed from the weak, medium and strong acid sites [38]. Since $Ni^{2+}$and Co^{3+} ratios are present in the catalyst, the catalyst acid densities can be attributed to the Co loading. In comparison with the 2%Co- $La_{0.2}Ca_{0.8}NiO_3$- ZrO_2, the TPD peak at 450 °C in the 0.5% Co- $La_1Ca_0NiO_3$- ZrO_2 reduced, while at 343 °C, the peak decreased, thus suggesting that the Co introduced as a result of low Ca content and high La, covered both the strong and medium acid sites in the 2%Co- $La_{0.2}Ca_{0.8}NiO_3$- ZrO_2 [38]. By increasing the Co loading from 1.5% Co- $La_{0.8}Ca_{0.2}NiO_3$- ZrO_2 to 2% Co- $La_{0.2}Ca_{0.8}NiO_3$- ZrO_2), the peak seen at 343 °C mimics those seen at 383 °C, while other peaks were seen to emerge at 450 °C and 600 °C. The peak intensities at 450 and 600 °C were seen to increase gradually with Co loading. Thus, the change in the electronic series of the perovskite catalyst affected the catalyst's activity and stability.

3.6. The CO_2-TPD results of the catalysts

Five desorption peaks of the CO_2-TPD at different temperatures are displayed in Fig. 6. Peak A (83 –100 °C), peak B (350–400 °C), and peak C (600–750 °C) are allotted to the presence of weak basic sites, intermediate basic sites and strong basic sites, respectively [37–39]. Since the strength of the CO_2 desorption peaks changed as the support composition of ZrO_2 changed, the amount of carbon dioxide desorbed from each site of the associated catalyst was determined. The amount of CO_2 desorbed gradually increased when the Co- $La_{1-x}Ca_xNiO_3$.ZrO_2 series catalysts' support characteristics changed, thus indicating a shift in the number of basic sites in the active sites of the catalyst. The initiation of different weight percents of Co led to the doubling of the number of basic sites. Therefore, the 2%Co- $La_{0.2}Ca_{0.8}NiO_3$- ZrO_2 displayed higher basic strength compared to those of the other analyzed catalysts in the DRM. Such enhanced basic strength might be linked to the interactions between Ni and Co on ZrO_2 support. Although, high Co content in the catalyst could be responsible for high alkaline content, other factors such as La contents in the 2%Co-La0.6Ca0.4NiO_3-ZrO_2 may have influenced the alkane sites of the catalyst as well as the Ca content in the perovskite, since they all have a substantial role to play in the catalyst. The basicity of a catalyst is influenced by chemical composition, local and bulk structure of the catalyst, metal interaction, chemical composition, and the nature of the surface species. [12,20]. Surface species can also influence the strength of the metal-oxygen link, thus leading to different types of basic sites. According to refs. [38–40], enhanced basicity yielded similar results. The removal of coke by the reaction of CO_2 with C to produce CO and the adsorption and conversion of additional CO_2 during the DRM reaction can both be improved by the presence of more basic sites [17,22].

3.7. XPS patterns of the Co- $La_{1-x}Ca_xNiO_3$.ZrO_2 perovskite catalysts

XPS shows oxygen species in O 1 s spectra after deconvolution (Fig. 7a-e). Lattice oxygen (O_{lat}) species have a peak at BE of 529.1–529.9 eV, while surface-adsorbed O_2 species (O_{ads}) have a peak at 530.5–531.0 eV [16,20] (Fig. 7a). Due to the ratio of O_{ads}/O_{lat}, the amount of surface O_2 species in 2% Co-$La_{0.2}Ca_{0.8}NiO_3$-ZrO_2 increased due to the Co and Ca loading in the perovskite, which changed its morphology and increased its oxidation stability, thus preventing the tendency for sintering and coke formation on the NiO catalysts. Fig. 7b displays the La 3d spectra of the Co-La_{1-x}CaxNiO_3-ZrO_2 perovskite catalyst. Each spin orbit component of La $3d_{3/2}$ and La $3d_{5/2}$ has a double peak. Shake-up satellites caused by intense O 2p → La 4 f charge transfer events or strong final state mixing of electronic configurations imposed the double peak [19]. Satellite peaks such as high-energy loss peaks were seen as $3d_{3/2}$ and $3d_{5/2}$ peaks [10,26]. The catalysts having energy intensities of 529.37 and 531.37 eV have low binding energy

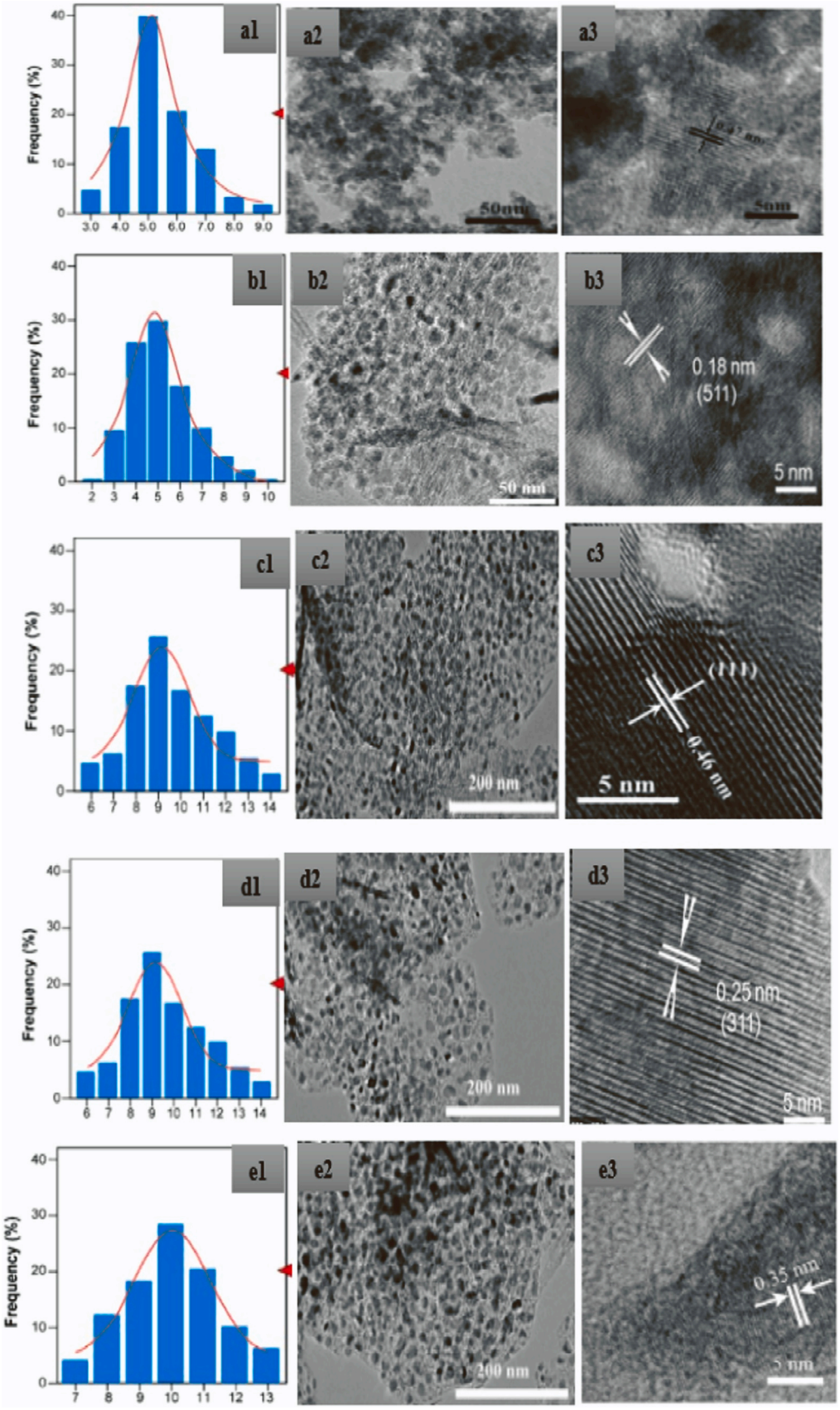

Fig. 3. Particle size distribution and TEM-sectional images of (a: a1–3) 2% Co- $La_{0.2}Ca_{0.8}NiO_3$- ZrO_2; (b: b1–3) 1.5%Co- $La_{0.4}Ca_{0.6}NiO_3$- ZrO_2; (c: c1–3) 2%Co- $La_{0.6}Ca_{0.4}NiO_3$- ZrO_2 (d: d1–3) 1.5% Co- $La_{0.8}Ca_{0.2}NiO_3$- ZrO_2; (e: e1–3) 0.5% Co- $La_1Ca_0NiO_3$- ZrO_2.

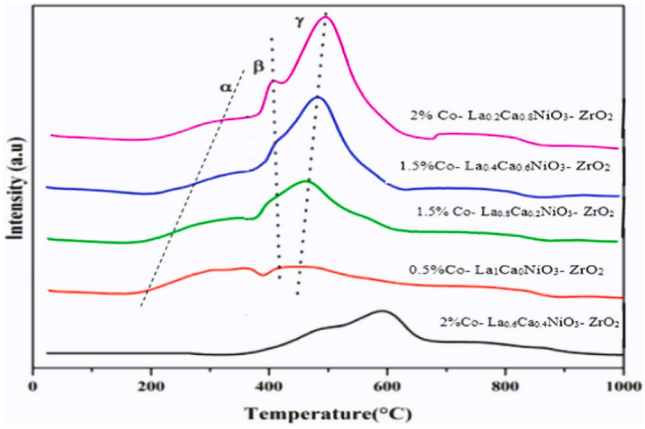

Fig. 4. H_2-TPR profiles of Co- $La_{1-x}Ca_xNiO_3$.ZrO_2 series catalysts.

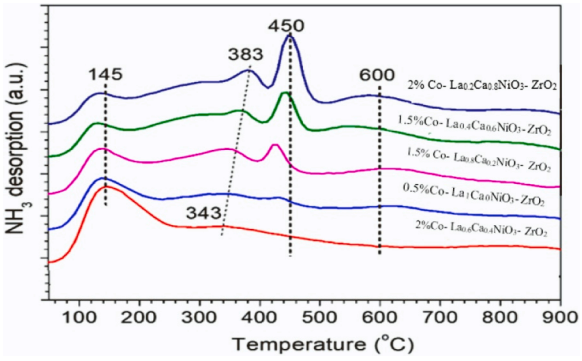

Fig. 5. NH_3-TPD profiles of Co- $La_{1-x}Ca_xNiO_3$.ZrO_2 series catalysts.

Table 2
The quantitative analysis of the degree of reduction of Ni during H_2-TPR.

Catalyst	Region of deduction			
	α − region (*μmol*/*g*)	*β − region* (*μmol*/*g*)	*γ − region* (*μmol*/*g*)	Total uptake (*μmol*/*g*)
2% Co- $La_{0.2}Ca_{0.8}NiO_3$- ZrO_2	107.5	271.4	636.1	1,015.0
1.5%Co- $La_{0.4}Ca_{0.6}NiO_3$- ZrO_2	91.3	137.5	191.2	420.0
2%Co- $La_{0.6}Ca_{0.4}NiO_3$- ZrO_2	56.6	100.4	166.1	323.1
1.5% Co- $La_{0.8}Ca_{0.2}NiO_3$- ZrO_2	38.3	79.5	99.0	216.8
0.5% Co- $La_1Ca_0NiO_3$- ZrO_2	30.9	69.8	79.9	186.6

compared to other catalysts, thus indicating that a percentage of La^{2+} is formed at the surface with increasing Ca due to Co loading. The results show that all the synthesized perovskite catalyst composites can dry-reform methane in the presence of CO_2, but the 2% Co-$La_{0.2}Ca_{0.8}$-NiO_3-ZrO_2 catalyst performed best due to its binding energy (Fig. 7c), which increased its activity and stability. The Ni-Co synergistic actions in the catalyst's lattice improved the catalyst's performance and reduced carbon deposition with a resultant high CO_2 and CH_4 conversion. When La is substituted in the perovskite with Ca, 2% Co- $La_{0.2}Ca_{0.8}NiO_3$- ZrO_2 showed the most significant sample-area decrease amongst all the

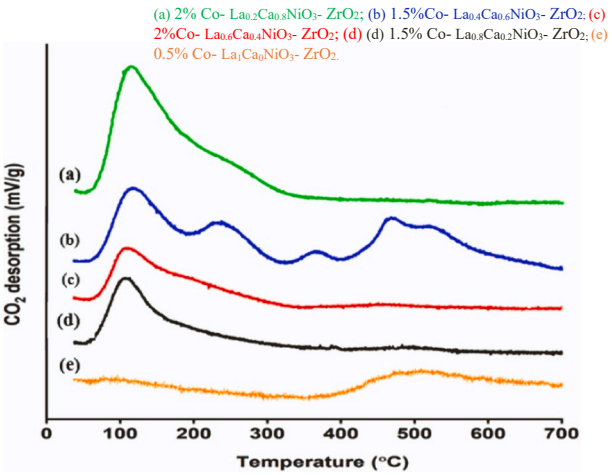

Fig. 6. CO_2-TPD profiles of Co- $La_{1-x}Ca_xNiO_3$.ZrO_2 series catalysts.

synthesized perovskites 9Figure 7b (a-e). The spin–orbit splitting between the $3d_{3/2}$ (528 eV) and $3d_{5/2}$ (536 eV) peaks correspond with those displayed in ref. [22], thus indicating the availability of quantities of active sites/interstices of La at the surface.

3.8. EDX analysis of 2% Co- $La_{0.2}Ca_{0.8}NiO_3$- ZrO_2 before and after the reaction

The Energy-dispersive X-ray spectroscopy (EDX) analysis of the catalysts before and after use in the DRM process, are presented in Fig. 8. These results show the elemental composition of the as-prepared catalyst and the used catalysts, which confirm the occurrence of all elemental constituents that were mixed together during the synthesis of the catalyst. Furthermore, the % loading of the elements of interest revealed by the EDX are the same as intended in the calculation and catalyst preparation with error values of ±4% and ±2% for Ni and La respectively.

3.9. Performance of the catalysts during the DRM reaction

By evaluating the catalyst's activities, the performance effects of the Co- $La_{1-x}Ca_xNiO_3$.ZrO_2 series were investigated. Fig. 9a-c depicts the calculated results for DRM at 700 °C for 60.0 h time-on-stream for CO_2 and CH_4 conversion (Figure 9b), H_2/CO mole ratio (Fig. 9c), and their selectivity. The 2% Co- $La_{0.2}Ca_{0.8}NiO_3$- ZrO_2 catalyst displayed higher and marginal CH_4, and CO_2 conversions compared to those of other catalysts during the DRM reaction. The improved surface area of the 2% Co- $La_{0.2}Ca_{0.8}NiO_3$- ZrO_2 enhanced the diffusion, adsorption and contact of the reactant gases. The high average pore volume and diameter of the 2% Co- $La_{0.2}Ca_{0.8}NiO_3$- ZrO_2, is a factor that influences the catalyst's high performance. The % loading of the catalyst on ZrO_2 support improved the activity of the catalyst. As shown in Fig. 9a, the 2% Co-$La_{0.2}Ca_{0.8}NiO_3$- ZrO_2 exhibited the highest catalyst activity i.e., (~88% methane and ~90% carbon dioxide conversion) among all the analyzed catalysts. The 1.5%Co- $La_{0.4}Ca_{0.6}NiO_3$- ZrO_2 also gave high CO_2 and CH_4 conversions, which is lower than that of the 2% Co- $La_{0.2}Ca_{0.8}NiO_3$-ZrO_2. The 2%Co- $La_{0.6}Ca_{0.4}NiO_3$- ZrO_2 did not show much activity in this regard. In terms of durability, the 2% Co- $La_{0.2}Ca_{0.8}NiO_3$- ZrO_2 displayed a high conversion and good stability. On the other hand, for the 0.5% Co- $La_1Ca_0NiO_3$- ZrO_2, 1.5%Co-$La_{0.8}Ca_{0.2}NiO_3$-ZrO_2 and 2% Co- $La_{0.6}Ca_{0.4}NiO_3$-ZrO_2, the catalyst's deactivation was very evident, with the conversion steadily declining within 30 h of time on stream (TOS) due to the presence of RWGS, the same trend was observed during its CO_2 conversion. It was observed that CO_2 conversion for all of the investigated catalysts was higher than that of methane which is indicative of the fact that RWGS was favoured in the catalysts' activities, thus

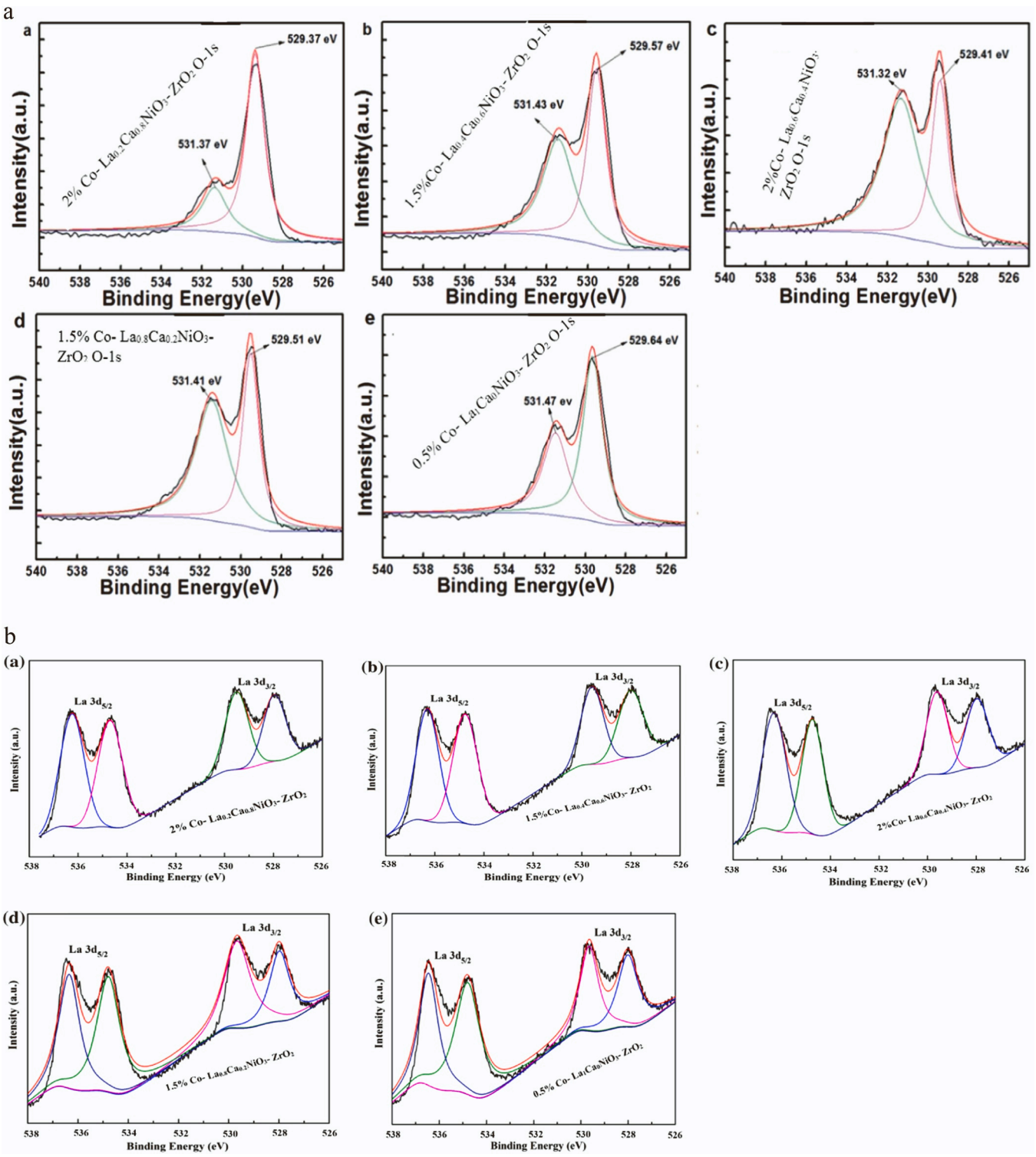

Fig. 7. a: O-1 s XPS of the perovskite catalysts (a) 2% Co- $La_{0.2}Ca_{0.8}NiO_3$- ZrO_2; (b) 1.5%Co- $La_{0.4}Ca_{0.6}NiO_3$- ZrO_2; (c) 2%Co- $La_{0.6}Ca_{0.4}NiO_3$- ZrO_2 (d) 1.5% Co- $La_{0.8}Ca_{0.2}NiO_3$- ZrO_2; (e) 0.5% Co- $La_1Ca_0NiO_3$- ZrO_2 b: La3d XPS of the perovskite catalysts (a) 2% Co- $La_{0.2}Ca_{0.8}NiO_3$- ZrO_2; (b) 1.5%Co- $La_{0.4}Ca_{0.6}NiO_3$- ZrO_2; (c) 2%Co- $La_{0.6}Ca_{0.4}NiO_3$- ZrO_2 (d) 1.5% Co- $La_{0.8}Ca_{0.2}NiO_3$- ZrO_2; (e) 0.5% Co- $La_1Ca_0NiO_3$- ZrO_2.

justifying the observations made in ref. [36].

$$CO + H_2O \leftarrow\rightarrow H_2 + CO_2 \Delta H_{298} = +41.2 kJ/mol \quad (3)$$

The forward reaction in Eq. 3 showing the WGS reaction favors more formation of CO_2 which is needed for the methane reforming reaction with H_2, however, the equilibrium conversion or highest conversion of CO_2 is attained as evident on the graphs from 30 to 60 h giving 90% conversion which also implies 10% of CO_2 is left unconverted owing to some reasons which are not far-fetched. For instance, as soon as the peak conversion of CO_2 is reached, it may imply minimal availability of water or total depletion of water molecules which may no longer the favor forward reaction. Hence, by the Lechatelier's principle, when there's an imposed constraint on a system undergoing reversible reaction, the equilibrium position of such a system shifts to annul the constraint; in

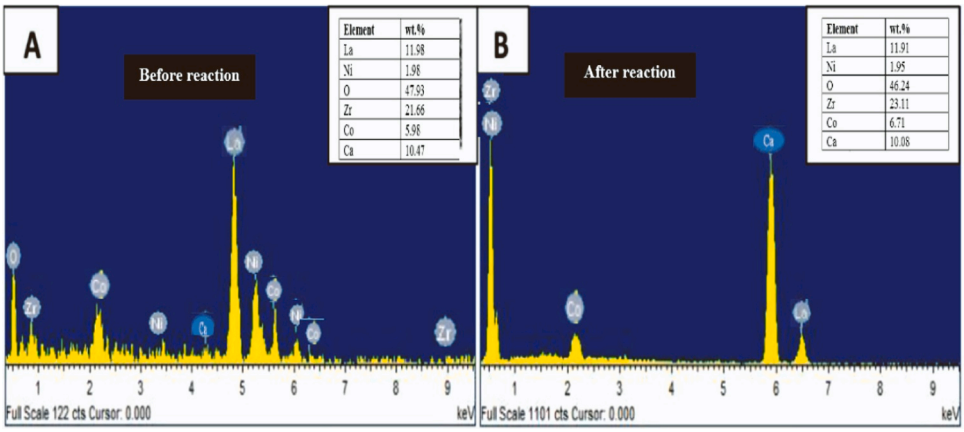

Fig.8. EDX analysis of 2% Co- $La_{0.2}Ca_{0.8}NiO_3$- ZrO_2: a. before and b. after the reaction.

this case, the constraint being peak conversion of CO_2 causes the equilibrium position to shift and in turn favor backward reaction. Again looking at the Reverse water gas shift reaction (RWGSR), the backward reaction favors the formation of CO which is a catalyst poisoner at the peak conversion of CO_2 obtained at 60 h, hence, catalyst deactivation may set in as a result of more/increased formation of CO, which may have deposited on the active sites of the catalyst and as such, a maximum of 90% CO_2 is attainable, that is, the reason why the catalysts/best catalyst was not able to attain 100% conversion of CO_2 is obviously as a result of catalyst-deactivation which may be caused by catalyst poisoning, ageing and coke deposition. However, the most prominent in this case is CO deposition/poisoning which competes for the active sites available for CO_2 in the perovskites.

As stated in the previous section, the CO_2 conversion is more than that of CH_4 when the H_2/CO mole ratio less than 1. Thus, for the 2% Co-$La_{0.2}Ca_{0.8}NiO_3$- ZrO_2 and 1.5%Co- $La_{0.4}Ca_{0.6}NiO_3$- ZrO_2, the H_2/CO ratio was stable as well at 0.88. But for the 2%Co- $La_{0.6}Ca_{0.4}NiO_3$- ZrO_2 and 0.5% Co- $La_1Ca_0NiO_3$- ZrO_2, the H_2/CO ratio decreased as the conversion dropped (Fig. 9c), thus signifying lower conversions.

*Methane conversion, CO_2 conversion and H_2/CO conversion values as a function of time on stream (TOS) for DRM.

Reaction conditions: 60 h, 700 ^oC, 1 atm. Catalyst amount is 30 mg. Reduced by pure H_2 at 800 ^oC for 1.5 h. N_2:CH_4: CO_2 = 1:1:1.

3.10. Hydrogen/carbon (II) oxide ratio at different temperatures

The reaction's H_2/CO ratio was measured and displayed in Fig. 10, which shows that this ratio increased as the temperature increased. As the reaction continued, the H_2/CO ratio was below 1 thus indicating a definite propensity towards the generation of water by the RWGS reaction [3,38]. This finding suggests that the synergistic effect of Ni and Co in the Co- $La_{1-x}Ca_xNiO_3$-ZrO_2 had restrained the RWGS reaction. According to the morphological analysis of the catalysts, the TEM images show that the bimetallic catalysts have more homogeneous distributions and well-defined active particle sizes which enhanced the surface-active areas for CO_2 activation and thus promoted the primary reaction (DRM). The H_2/CO ratios ranged from 0.40 to 0.88, which was adequate for the F-T synthesis.

3.11. Deactivation rate and carbon deposition of Co- $La_{1-x}Ca_xNiO_3$-ZrO_2 series catalysts

The carbon deposition and deactivation rates of the Co- $La_{1-x}Ca_x$-NiO_3-ZrO_2 series catalysts are given in Table 3. The values were calculated using the equilibrated mixture method. A few of the Co-$La_{1-x}Ca_xNiO_3$-ZrO_2 series catalysts displayed good activities throughout the tests, however, they steadily deactivated over the course of their 60-h time on-stream. When compared to other catalysts, the 2%Co-$La_{0.2}Ca_{0.8}NiO_3$-ZrO_2 catalyst had the maximum CO_2 conversion of 90%, with an initial CO_2 conversion of around 80.6%. Based on these findings, the synergistic effects of the two metals may keep up with or even speed up the quick conversion of surface-active intermediates, which had less of an impact on the catalyst's activity at first. Remarkably, the stability of the 2% Co- $La_{0.2}Ca_{0.8}NiO_3$- ZrO_2 catalyst was obviously higher than those of other catalysts as observed for the DRM. The varied synergetic effects of these catalysts may be responsible for the differences in the catalysts' performances, which resulted in the significant structural differences that were already recounted in the preceding sections. The intermetallic Ni-Co composite of the 2%Co-$La_{0.2}Ca_{0.8}NiO_3$-ZrO_2 catalyst is very active for methane decomposition. However, the intermetallic Ni-Co sites had close contact with the basic/redox support site as a result of the SMSI effect, which also stimulated the rapid removal of carbon intermediates that occurred during the decomposition of CH_4 [30–33]. For example, several researchers proposed that the deposition of carbon during reforming depends greatly on the nature of bimetallic catalyst and carbon particles which are formed on larger metal particles where the graphitization of carbon is preferred [25,29,33,38]. However, the 2%Co- $La_{0.2}Ca_{0.8}NiO_3$-ZrO_2 catalyst exhibited higher porosity and good pore structure among others, which in turn enhanced the coking resistance of the catalyst. Based on the TPR plots, the 2%Co-$La_{0.6}Ca_{0.4}$-NiO_3-ZrO_2 and 0.5%Co-$La_1Ca_0NiO_3$-ZrO_2 showed relatively few free metal particles within their lattices. This may considerably reduce the possibility of coking and deactivation at the catalysts' active sites. Some authors recently reported that doping the right amounts of Co into a Ni-based catalyst is feasible to help speed up CH_4 decomposition [37–39]. Since the production and removal rates of the carbon intermediates were best matched by the optimized Ni-Co interactions and metal-support interactions offered by the best catalyst, the 2% Co-$La_{0.2}Ca_{0.8}NiO_3$-ZrO_2 catalyst in turn displayed the best stability and activity.

3.12. Carbon deposition over the spent catalysts

Three factors are typically responsible for the catalysts' deactivation in DRM environments. These include (i) oxidation of metal sites [24]; (ii) metal sintering [7,28], (iii) carbon deposition. All the spent catalysts had carbon deposited on them. Although the appearance of carbon deposits is the reason why catalysts become inactive, the ZrO_2 support and the Perovskite-type oxides helped to prevent this from happening, thus reducing coke formation. Additionally, the observed TGA profiles of the catalysts revealed the existence of minimal filamentous carbon in the catalysts' framework. Therefore, the sole explanation for the earlier deactivation of the 2%Co-$La_{0.6}Ca_{0.4}NiO_3$-ZrO_2, 0.5% Co- $La_1Ca_0NiO_3$-ZrO_2, and 1.5%Co-$La_{0.8}Ca_{0.2}NiO_3$-ZrO_2 is as a result of metal site

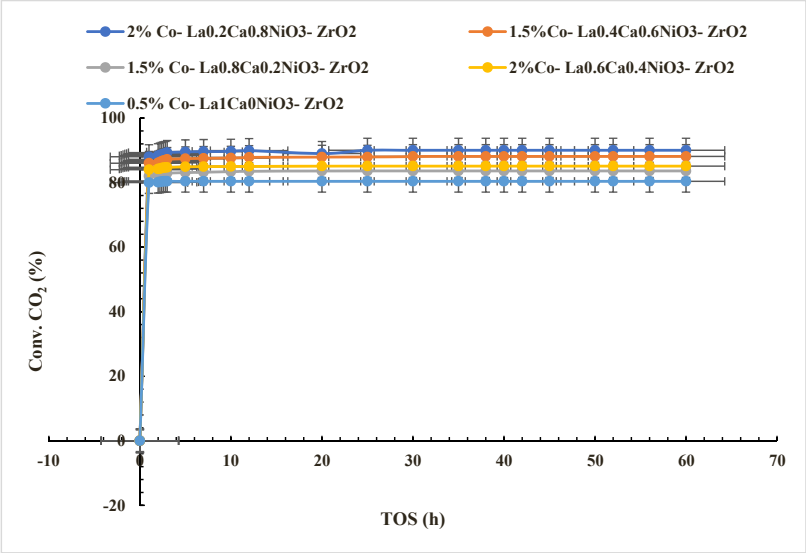

(a)

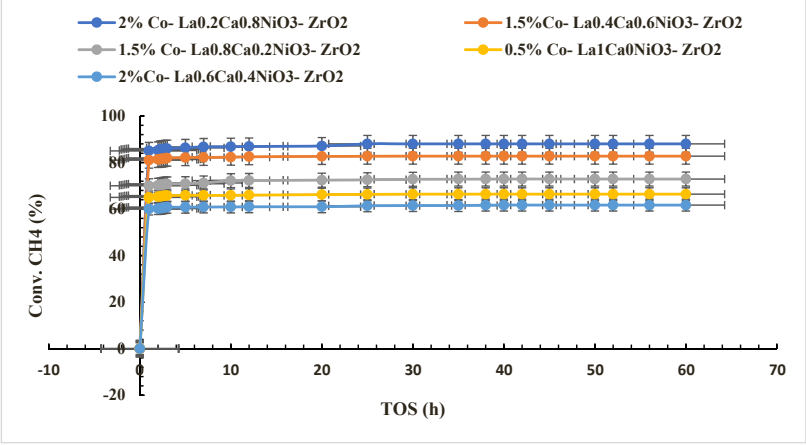

(b)

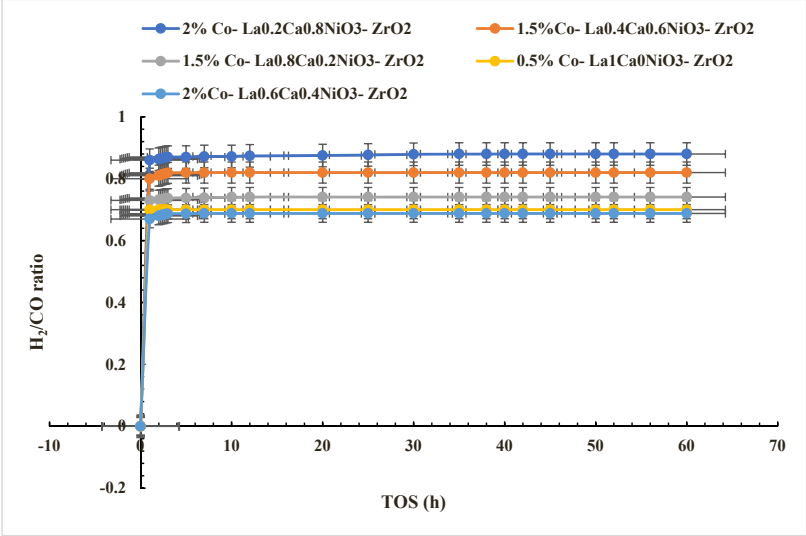

(c)

Fig. 9. Conversion of: a. CO_2, b. CH_4 and, c. H_2/CO ratio at varying TOS.

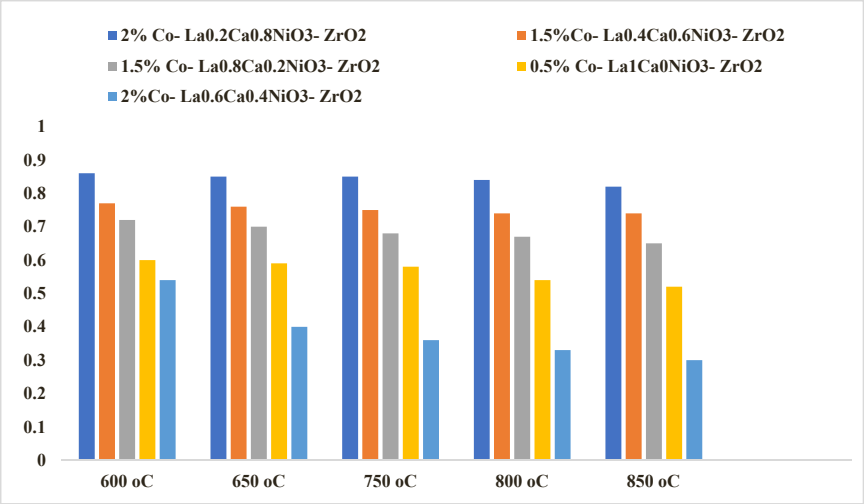

Fig. 10. H_2/CO ratios of the catalyst at various temperatures.

Table 3
Carbon deposition and deactivation rate of Co- $La_{1-x}Ca_xNiO_3.ZrO_2$ series catalysts.

Catalyst	Carbon deposit (g_c. $gcat^{-1}$)	Coking rate ($mg_c.g^{-1}_{cat}h^{-1}$)
0.5% Co- $La_1Ca_0NiO_3$- ZrO_2	0.130	7.04
1.5% Co- $La_{0.8}Ca_{0.2}NiO_3$- ZrO_2	0.033	4.63
2%Co- $La_{0.6}Ca_{0.4}NiO_3$- ZrO_2	0.139	9.44
1.5%Co- $La_{0.4}Ca_{0.6}NiO_3$- ZrO_2	0.029	3.98
2% Co- $La_{0.2}Ca_{0.8}NiO_3$- ZrO_2	0.003	1.01

Catalytic behavior of catalyst after 60 h of reaction at 700 °C

oxidation, which is frequently seen in Co catalysts [41–43]. For the spent 1.5%Co-$La_{0.4}Ca_{0.6}NiO_3$-ZrO_2 catalyst and most importantly, the 2%Co-$La_{0.2}Ca_{0.8}NiO_3$- ZrO_2, they displayed minute carbon deposition even after 60 h TOS, thus demonstrating excellent carbon resistance, which is in line with the results obtained from TGA. The Boudouard reaction, which is also in charge of lowering the catalyst's performance, is the cause of the carbon deposits that were found on the surface of the spent catalysts; similar conclusions were drawn by refs. [10,24]. They reported that carbon deposition would be suppressed by the potent electronic interaction between the finely dispersed metals and the catalyst support. After the 60-h period of reaction, a quantitative analysis was carried out to quantify the carbon deposits on the spent catalysts. All the catalysts showed significant weight losses between 200 and 800 °C, with constant weights at 800 °C. The two most reactive catalysts (i.e., the 2% Co- $La_{0.2}Ca_{0.8}NiO_3$- ZrO_2 **(A)** and 1.5%Co- $La_{0.4}Ca_{0.6}NiO_3$- ZrO_2 **(D)**) displayed minute quantities of carbon deposition with corresponding weight loss of 16.0% based on the TGA profiles, which showed that they had higher weight losses relative to other catalysts. The perovskite type **C** showed mild weight loss. The TGA results revealed that the combined metal catalysts i.e., the 2%Co-$La_{0.2}Ca_{0.8}NiO_3$- ZrO_2 **(E)** and 1.5%Co-$La_{0.4}Ca_{0.6}NiO_3$- ZrO_2 **(D)** (Fig. 11), had a significant increase in the catalysts' capacity for feed conversion and hence, gasified the carbon deposits on their surfaces. The catalysts' distribution, Co loading, surface areas and active sites, may be responsible for this, hence the low buildup of carbon deposits on the surface of both catalysts is responsible for their lower weight measurements whereas, others with added carbon deposits on their surfaces recorded higher weights.

ZrO_2; **D** . 1.5%Co- $La_{0.4}Ca_{0.6}NiO_3$- ZrO_2; **E** - 2% Co- $La_{0.2}Ca_{0.8}NiO_3$-ZrO_2.

Table 4 gives the calculated carbon balances of the tested catalysts [28]. The reactor's carbon mass was computed based on the overall amount of reactant fed during the process. The reactor output mass of carbon was determined by adding the carbon deposit mass from thermographic analysis, outlet in liquid phase, and product gases from GC-MS analysis. The results show that the 2%Co- $La_{0.2}Ca_{0.8}NiO_3$-ZrO_2 achieved a Carbon balance greater than 98.978% because Co, La and Ca additive with the support of Zr helped to reduce carbon deposition.

Upon subjecting the samples to TGA analysis the % reduction in

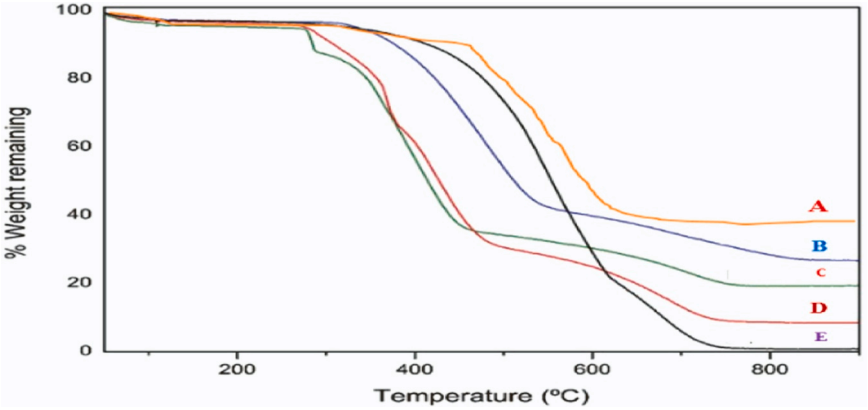

Fig. 11. Weight loss (TG %) curves of Co- $La_{1-x}Ca_xNiO_3.ZrO_2$ series catalysts. Legend:2%Co- $La_{0.6}Ca_{0.4}NiO_3$- ZrO_2; **B** - 0.5% Co- $La_1Ca_0NiO_3$- ZrO_2; **C**- 1.5% Co-$La_{0.8}Ca_{0.2}NiO_3$-.

Table 4
Carbon (C) balance calculation.

Perovskite catalysts	C_{feed} in the reactor (g)[a]	C_{outlet} in the liquid phase (g)[b]	C_{outlet} in the solid phase (g)[c]	C_{outlet} in the gas phase (g)[d]	Overall carbon balance (%)
2%Co- $La_{0.2}Ca_{0.8}NiO_3$-ZrO_2	318.698	77.885	0.199	239.291	99.699

[a]mass of C fed into the reactor
[b]mass of C outlet in the liquid phase
[c]mass of C outlet in the solid phase
[d]mass of C outlet in the gas phase

weight as a result of moisture loss is as documented in Table 5, which showed the fresh catalyst, weight of catalyst after 60 h of reaction, weight gain, % moisture removed from the catalyst during TGA, weight of water loss and weight of catalyst after dehydration as obtained from TGA.

3.13. Surface oxygen vacancy (SOV) and activation of CO_2

Active sites for CO_2 activation have been reported to be dominated by oxygen vacancies (OVs) on metal oxides [6]. Binding sites for surface-adsorbed species or traps for excited electronic charges can be provided by these vacancies. Surface oxygen vacancies (OVs) help to enhance the effectiveness of charge transfer processes and the reduction of carbon dioxide activation energy by providing extra electrons that can adsorb onto carbon dioxide molecules and activate them. Based on this, one may consider the most active catalyst (2% Co- $La_{0.2}Ca_{0.8}NiO_3$- ZrO_2) to have the capacity to produce OVs with the least amount of work, hence one can conclude that carbon dioxide activation on OVs is the step involved in determining the reaction rate (Fig. 12). Due to high O_2 and unoccupied mobile $LaNiO_3$ interface in the Co, 2% Co- $La_{0.2}Ca_{0.8}NiO_3$-ZrO_2, it exhibited greater methanation selectivity and activity. These phases of the mechanism take place on the same active sites, which is a drawback for employing different catalysts, as there may be tendencies for the coke buildup on these active sites, which may in turn delay the chemisorption of additional CO_2 molecules. Hollow CeO_2 microspheres with a Ni-based catalyst support and La doping were produced by Zhang et al. [44]. Due to its higher OVs, which were essential in the generation of CH_4, the La-doped CeO_2 catalyst gave the best performance during the methanation of CO_2 when compared to other catalysts. The carbon dioxide (CO_2) molecules react with the O_2 vacant sites (active O sites) at the Ni-CeO2-La interface after adsorption onto the Ni/CeO_2-La-600, thus yielding OCO_2*. The steps were repeated as many times as necessary in order to achieve the targeted OCO_2 concentration. The newly formed OCO_2* reacts with the released H to form hydrogenated carbonates, which may be further hydrogenated to yield methane via several intermediate species. Hao et al. [45] studied how surface oxygen vacancies and nickel particle size affected the methanation of carbon dioxide over Ni- CeO_2. The occurrence of SOVs caused by the synergy of CeO_2 and Ni resulted in increased selectivity for methane, higher conversion rates, and lower activation energies in comparison to the results obtained with Ni/SiO_2.

The activity of most of the previously reported Ni-based catalysts for DRM reaction are presented in Table6.

4. Conclusion

Series of Co-$La_{1-x}Ca_xNiO_3$.ZrO_2 catalysts were successfully prepared by co-precipitation method and the performance of the catalysts were examined during their DRM reactions. The H_2-TPR analysis showed that the catalysts require higher temperatures for the reduction reactions. At the end of the reduction process, the perovskite structure disintegrated, thus resulting in the production of Co particles ingrained in the perovskite matrix. The 2%Co-$La_{0.2}Ca_{0.8}NiO_3$-ZrO_2 displayed excellent activity and stability as well as the highest rate of methane conversion compared to other catalysts. The inclusion of Co in the catalyst's framework accelerated the oxidation of deposited carbon to carbon monoxide, thus increasing the catalyst's activity and stability. Furthermore, the bimetallic catalyst influenced the intrinsic properties such as nano-crystalline and mesoporous frameworks and highly dispersed metal sites. Nevertheless, different characteristics were observed in relation to the physicochemical properties of the catalysts owing to the difference in Co loading which induced the varying synergetic effects that were evident in the catalysts. In the case of the 2%Co-$La_{0.2}Ca_{0.8}NiO_3$-ZrO_2 catalyst, the coexisting Co species formed a homogenous framework that resulted in a stable and strong metal support interaction. The variation in the catalyst's stability and activity suggests that the metal-support interactions and metal synergy were crucial for the catalyst's successful operation. The 2%Co- $La_{0.2}Ca_{0.8}NiO_3$-ZrO_2 gave the best performance and coke resistance due to the optimized synergy of the metal-metal contact and metal-support interaction which gave the best match of carbon intermediate formation as well as its elimination compared to others. Several catalysts were used including the 2%Co-$La_{0.6}Ca_{0.4}NiO_3$-ZrO_2, 0.5%Co-$La_1Ca_0NiO_3$-ZrO_2, and 1.5%Co- $La_{0.8}Ca_{0.2}NiO_3$-ZrO_2. However, it was observed that the catalysts brought in the generated carbon intermediate, which had the potential to generate inert graphitic carbon and thus increased the propensity for catalyst deactivation. Despite having the lowest pore volume (2.37 cm^3/g), the 2% Co-$La_{0.2}Ca_{0.8}NiO_3$- ZrO_2, possessed highly dispersed particles, which is essential for its good stability, surface characteristics and activity with improved characteristics as imposed by the Ni-Co synergy when

Table 5
Weight gain and loss of catalyst as a result of dehydration during TGA.

Catalyst	Fresh catalyst wt. (g)	Wt. of cat. After 60 h of reaction (g)	Weight gain (g)	% moisture removed from cat. during TGA	Wt. of water loss during TGA	Weight of cat after dehydration as obtained from TGA (g)
2%Co- $La_{0.6}Ca_{0.4}NiO_3$-ZrO_2;	0.1	0.110	0.010	99.504	99.504% of 0.01 g = 0.0099504 g	0.1000496
0.5% Co- $La_1Ca_0NiO_3$-ZrO_2	0.1	0.109	0.009	99.593	99.593% of 0.009 g =	0.1000366
1.5% Co-$La_{0.8}Ca_{0.2}NiO_3$- ZrO_2	0.1	0.107	0.007	98.995	98.995% of 0.007 g = 0.1006 g	0.1000704
1.5%Co-$La_{0.4}Ca_{0.6}NiO_3$-ZrO_2;	0.1	0.106	0.006	99.569	99.569% of 0.006 g = 0.1004 g	0.1000259
2% Co-$La_{0.2}Ca_{0.8}NiO_3$- ZrO_2	0.1	0.104	0.004	99.699	99.699% of 0.004 g = 0.1002 g	0.1000120

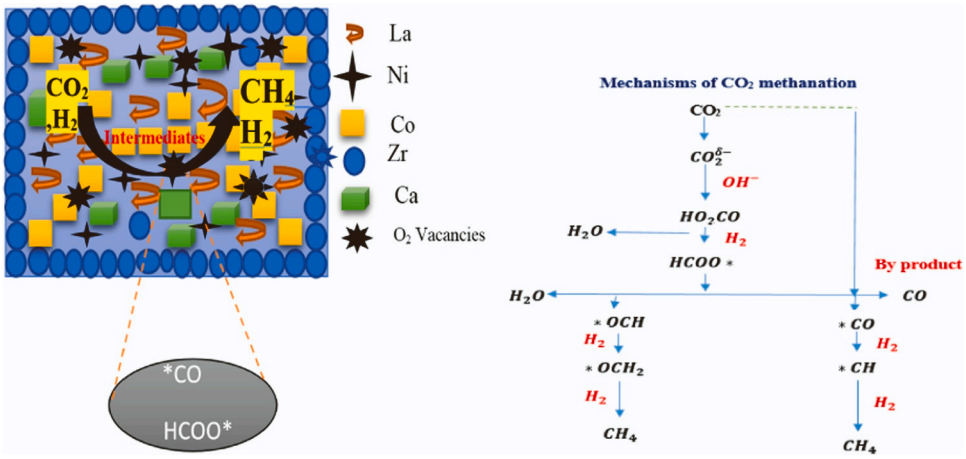

Fig. 12. Methanation of CO_2 over 2%Co- $La_{0.2}Ca_{0.8}NiO_3$-ZrO_2 depends on OVs.

Table 6
Compared performances of different catalysts for DRM reaction from previous works and this study.

	Reaction conditions				Conversion %			
Catalyst	**% Ni loading**	**Temp (°C)**	**CH_4: CO_2:N_2(Ar)**	**GHSV/h^{-1}**	**CH_4**	**CO_2**	**H_2/CO**	**Refs.**
1%Ni/10%La-ZrO_2	1	150	1:1:2	-	74.5	83.5	0.83	[46]
Ni-CaO/La_2O_3-ZrO_2	5	450	1:1:1	5882	9.8	12.9	-	[47]
Pt/Ni/Mg/$Ce_{0.6}Zr_{0.4}O_2$	8	454	7:7:86	68000	10	10	0.23	[48]
5% Ni/$Ce_{0.6}Zr_{0.4}O_2$	5	650	1:1:0	37600	53	53	0.92	[49]
$CeNi_{0.9}Zr_{0.01}Y_{0.09}O_3$	1	800	-	42000	85	90	> 1	[50]
$La_{0.6}Ce_{0.4}Ni_{0.9}Zr_{0.1}O_3$	1	800	1:1:0	42000	86	90	1	[51]
2%Co- $La_{0.2}Ca_{0.8}NiO_3$-ZrO_2	2	700	1:1:1	42000	88	90	1	This study

compared to others.

CRediT authorship contribution statement

Babalola Aisosa Oni: Conceived the idea, carried out the experimentation, Made the first draft copy of the manuscript and Result analyses. **Samuel Eshorame Sanni:** Made useful contributions at different stages of the research and data curation; **Victor Oyebamiji Ojo:** General editing of manuscript. **Olusegun Stanley Tomomewo:** Made very vital/useful observations at the experimental design and experimentation.

Declaration of Competing Interest

The authors declare that they have no known competing financial interests or personal relationships that could have appeared to influence the work reported in this paper.

Data availability

No data was used for the research described in the article.

References

[1] A.S. Al-Fatesh, R. Patel, V.K. Srivastava, A.A. Ibrahim, M.A. Naeem, A.H. Fakeeha, A.E. Abasaeed, A.A. Alquraini, R. Kumar, Barium-Promoted Yttria–Zirconia-Supported Ni Catalyst for Hydrogen Production via the Dry Reforming of Methane: Role of Barium in the Phase Stabilization of Cubic ZrO_2, ACS Omega 7 (19) (2022) 16468–16483, https://doi.org/10.1021/acsomega.2c00471.

[2] X. Zhu, P. Huo, Y.P. Zhang, D.G. Cheng, C.J. Liu, Structure and reactivity of plasma treated Ni/Al_2O_3 catalyst for CO_2 reforming of methane, Appl. Catal. B: Environ. 81 (2008) 132–140.

[3] J.R. Rostrup-Nielsen, J. Sehested, J.R. Norskov, Hydrogen and synthesis gas by steam- and CO_2 reforming, Adv. Catal. 47 (2002) 65–139.

[4] Y. Kathiraser, W. Thitsartarn, K. Sutthiumporn, S. Kawi, Inverse $NiAl_2O_4$ on $LaAlO_3$–Al_2O_3: unique catalytic structure for stable CO_2, Reform. methane, J. Phys. Chem. C. 117 (2013) 8120–8130.

[5] J. Guo, H. Lou, H. Zhao, D. Chai, X. Zheng, Dry reforming of methane over nickel catalysts supported on magnesium aluminate spinels, Appl. Catal., A 273 (2004) 75–82.

[6] N.A. Pechimuthu, K.K. Pant, S.C. Dhingra, R. Bhalla, Characterization and activity of K, CeO_2, and Mn promoted Ni/Al_2O_3 catalysts for carbon dioxide reforming of methane, Ind. Eng. Chem. Res. 45 (2006) 7435–7443.

[7] J. Zhang, 2008. Research and Development of Ni Based Catalysts for CO2 Reforming of Methane. PhD Thesis. Department of Chemical Engineering, University of Saskatchewan, Saskatoon.

[8] J. Zhang, H. Wang, A.K. Dalai, Kinetic studies of carbon dioxide reforming of methane over Ni_Co/Al_Mg_O bimetallic catalyst, Ind. Eng. Chem. 48 (2009) 677–684.

[9] Y.H. Wang, H.M. Liu, B.Q. Xu, Durable Ni/MgO catalysts for CO_2 reforming of methane: activity and metal-support interaction, J. Mol. Catal. Chem. 299 (2009) 44–52.

[10] S. Assabumrungrat, S. Charoenseri, N. Laosiripojana, W. Kiatkittipong, P. Praserthdam, Effect of oxygen addition on catalytic performance of Ni/ SiO_2 MgO toward carbon dioxide reforming of methane under periodic operation, Int. J. Hydrog. Energy 34 (2009) 6211–6220.

[11] G.R. Moradi, M. Rahmanzadeh, S. Sharifnia, Kinetic investigation of CO_2 reforming of CH_4 over La–Ni based perovskite, Chem. Eng. J. 162 (2010) 787–791.

[12] C.S. Song, W. Pan, S.T. Srimat, J. Zheng, Y. Li, Y.H. Wang, B.Q. Xu, Q.M. Zhu, Tri-reforming of methane over Ni catalysts for CO_2 conversion to syngas with desired H_2/CO ratios using flue gas of power plants without CO_2 separation, Stud. Surf. Sci. Catal. 153 (2004) 315–322.

[13] A. Slagtern, U. Olsbye, R. Blom, I.M. Dahl, The influence of rare earth oxides on Ni/ Al2O3 catalysts during CO_2 reforming of, Stud. Surf. Sci. Catal. 107 (497–502) (1997) CH4.

[14] H. Long, Y. Xu, X. Zhang, S. Hu, S. Shang, Y. Yi, X. Dai, Ni-Co/Mg-Al catalyst derived from hydrotalcite-like compound prepared by plasma for dry reforming of methane, J. Energy Chem. 22 (2013) 733–739.

[15] A.S. Al-Fatesh, N. Patel, A.H. Fakeeha, M.F. Alotibi, S.B. Alreshaidan, R. Kumar, Reforming of methane: effects of active metals, supports, and promoters, Catal. Rev. (2023) 1–99.

[16] H.O. Seo, J.K. Sim, K.D. Kim, Y.D. Kim, D.C. Lim, S.H. Kim, Carbon dioxide reforming of methane to synthesis gas over a TiO_2-Ni inverse catalyst, Appl. Catal. A Gen. 451 (2013) 43–49, https://doi.org/10.1016/j.apcata.2012.10.037.

[17] J.L. Rogers, M.C. Mangarella, A.D. D'Amico, J.R. Gallagher, M.R. Dutzer, E. Stavitski, J.T. Miller, C. Sievers, Differences in the nature of active sites for methane dry reforming and methane steam reforming over nickel aluminate

catalysts, ACS Catal. 6 (2016) 5873–5886, https://doi.org/10.1021/acscatal.6b01133.
[18] A. Abasaeed, S. Kasim, W. Khan, M. Sofiu, A. Ibrahim, A. Fakeeha, A. Al-Fatesh, Hydrogen yield from CO_2 reforming of methane: impact of La2O3 doping on supported Ni catalysts, Energies 14 (9) (2021) 2412.
[19] Y. Wang, A. Zhu, Y. Zhang, C.T. Au, X. Yang, Chuan Shi, Catal. Reduct. NO CO NiO/CeO2 Catal. Stoichiom. NO/CO NO/CO/O2 React. 81 (1–2) (2008) 141–149, https://doi.org/10.1016/j.apcatb.2007.12.005.
[20] R. Kumar, K. Kumar, N.V. Choudary, K.K. Pant, Effect of support materials on the performance of Ni-based catalysts in tri-reforming of methane, Fuel Process. Technol. 186 (2019) 40–52.
[21] X. You, J. Wang, W. Xiang, Y. Ma, J. Liu, W. Liu, X. Xu, H. Peng, C. Li, W. Zhou, P. Yuan, X. Chen, Ni-Co/Al_2O_3 bimetallic catalysts for CH_4 steam reforming: elucidating the role of Co for improving coke resistance, ChemCatChem (2014), https://doi.org/10.1002/cctc.201402695.
[22] I.V. Yentekakis, G. Goula, P. Panagiotopoulou, A. Katsoni, E. Diamadopoulos, D. Mantzavinos, A. Delimitis, Dry reforming of methane: catalytic performance and stability of Ir catalysts supported on γ-Al2O3, Zr0.92Y0.08O2-δ (YSZ) or Ce0.9Gd0.1O2-δ (GDC) supports, Top. Catal. 58 (2015) 1228–1241.
[23] D. San José-Alonso, M.J. Illán-Gómez, M.C. Román-Martínez, Low metal content Co and Ni alumina supported catalysts for the CO_2 reforming of methane, Int. Jou Hyd Energy 38 (5) (2013) 2230–2239, https://doi.org/10.1016/j.ijhydene.2012.11.080.
[24] G. Valderrama, A. Kiennemann, M.R. Goldwasser, Dry. Reform. CH_4 Solid Solut. $LaNi_{1-x}CoxO_3$ 133–135 (none) (2008) 142–148, https://doi.org/10.1016/j.cattod.2007.12.069.
[25] G.S. Gallego; C. Batiot-Dupeyrat; J. Barrault; E. Florez; F. Mondragón (2008). Dry reforming of methane over LaNi1yByO3d (B = Mg, Co) perovskites used as catalyst precursor., 334(1–2), 251–258.
[26] J. Ni, L. Chen, J. Lin, M.K. Schreyer, Z. Wang, S. Kawi, High performance of Mg– La mixed oxides supported Ni catalysts for dry reforming of methane: the effect of crystal structure, Int. J. Hydrog. Energy 38 (2013) 13631–13642.
[27] E. Akpan, Y. Sun, P. Kumar, H. Ibrahim, A. Aboudheir, R. Idem, Kinetics, experimental and reactor modeling studies of the carbon dioxide reforming of methane (CDRM) over a new Ni/CeO $_2$–ZrO_2 catalyst in a packed bed tubular reactor, Chem. Eng. Sci. 62 (2007) 4012–4024.
[28] M.S. Zanuttini, M.A. Peralta, C.A. Querini, Deoxygenation of m-cresol: deactivation and regeneration of Pt/γ-Al2O3 catalysts, Ind. Eng. Chem. Res. 54 (2015) 4929–4939.
[29] Y. Kathiraser, Z. Wang, S. Kawi, Oxidative CO_2 reforming of methane in $La_{0.6}Sr_{0.4}Co_{0.8}Ga_{0.2}O_{3-}$d (LSCG) hollow fiber membrane reactor, Environ. Sci. Technol. 47 (2013) 14510–14517.
[30] E.L. Gubanova, Y. Schuurman, V.A. Sadykov, C. Mirodatos, A.C. van Veen, Evaluation of kinetic models for the partial oxidation of methane to synthesis gas over a Pt/PrCeZrOx catalyst coated on a triangular monolith, Chem. Eng. J. 154 (2009) 174–184.
[31] C. Shi, P. Zhang, Role of MgO over g-Al_2O_3-supported Pd catalysts for carbon dioxide reforming of methane, Appl. Catal., B 170–171 (2015) 43–52.
[32] S.A. Theofanidis, R. Batchu, V.V. Galvita, H. Poelman, G.B. Marin, Carbon gasification from Fe-Ni catalysts after methane dry reforming, Appl. Catal. B 185 (2016) 42–55.
[33] E.H. Yang, N.Y. Kim, Y.S. Noh, S.S. Lim, J.S. Jung, J.S. Lee, G.H. Hong, D.J. Moon, Steam CO_2 reforming of methane over La1-xCexNiO_3 perovskite catalysts, Int. J. Hydrog. Energy 40 (2015) 11831–11839.
[34] J.W. Han, C. Kim, J.S. Park, H. Lee, Highly coke-resistant Ni nanoparticle catalysts with minimal sintering in dry reforming of methane, ChemSusChem 7 (2) (2014) 451–456, https://doi.org/10.1002/cssc.201301134.
[35] M.-S. Fan, A.Z. Abdullah, S. Bhatia, Catalytic technology for carbon dioxide reforming of methane to synthesis gas, ChemCatChem 1 (2009) 192–208.
[36] K. Nagaoka, K. Takanabe, K.-i Aika, Modification of Co/TiO_2 for dry reforming of methane at 2 MPa by Pt, Ru or Ni, Appl. Catal. A 268 (2004) 151–158.
[37] M.V. Sivaiah, S. Petit, J. Barrault, C. Batiot-Dupeyrat, S. Valange, CO_2 reforming of CH_4 over Ni-containing phyllosilicates as catalyst precursors, Catal. Today 157 (2010) 397–403.
[38] J. Hu, H. Poelman, G.B. Marin, C. Detavernier, S. Kawi, V.V. Galvita, FeO controls the sintering of iron-based oxygen carriers in chemical looping CO_2 conversion, J. CO_2 Util. 40 (2020), 101216.
[39] H. Peng, X. Zhang, X. Han, X. You, S. Lin, H. Chen, W. Liu, X. Wang, N. Zhang, Z. Wang, P. Wu, H. Zhu, S. Dai, Catalysts in coronas: a surface spatial confinement strategy for high-performance catalysts in methane dry reforming, ACS Catal. 9 (2019) 9072–9080, https://doi.org/10.1021/acscatal.9b00968.
[40] S. Arora, R. Prasad, An overview on dry reforming of methane: strategies to reduce carbonaceous deactivation of catalysts, RSC Adv. 6 (2016) 108668–108688, https://doi.org/10.1039/c6ra20450c.
[41] L. Wang, F. Wang, Design strategy, synthesis, and mechanism of ni catalysts for methane dry reforming reaction: recent advances and future perspectives, Energy Fuels 36 (11) (2022) 5594–5621, https://doi.org/10.1021/acs.energyfuels.2c01007.
[42] I. Hussain, G. Tanimu, S. Ahmed, C.U. Aniz, H. Alasiri, K. Alhooshani, A review of the indispensable role of oxygen vacancies for enhanced CO_2 methanation activity over CeO2-based catalysts: uncovering, influencing, and tuning strategies, Int. J. Hydrog. Energy (2022).
[43] H. Yang, Y. Zeng, Y. Zhou, X. Du, D. Li, C. Hu, One-step synthesis of highly active and stable Ni-ZrO2 catalysts for the conversion of methyl laurate to alkanes, J. Catal. 413 (2022) 297–310.
[44] T. Zhang, W. Wang, F. Gu, W. Xu, J. Zhang, Z. Li, T. Zhu, G. Xu, Z. Zhong, F. Su, Enhancing the low-temperature CO_2 methanation over Ni/La-CeO2 catalyst: The effects of surface oxygen vacancy and basic site on the catalytic performance, Appl. Catal. B: Environ. 312 (2022), 121385.
[45] Z. Hao, J. Shen, S. Lin, X. Han, X. Chang, J. Liu, M. Li, X. Ma, Decoupling the effect of Ni particle size and surface oxygen deficiencies in CO_2 methanation over ceria supported Ni, Appl. Catal. B: Environ. 286 (2021), 119922.
[46] T. Yabe, K. Mitarai, K. Oshima, S. Ogo, Y. Sekine, Low-temperature dry reforming of methane to produce syngas in an electric field over La-doped Ni/ZrO2 catalysts, Fuel Process. Technol. 158 (2017) 96–103.
[47] B. Bachiller-Baeza, C. Mateos-Pedrero, M.A. Soria, A. Guerrero-Ruiz, U. Rodemerck, I. Rodríguez-Ramos, Transient studies of low-temperature dry reforming of methane over Ni-CaO/ZrO2-La2O3, Appl. Catal. B Environ. 129 (2013) 450–459.
[48] N.H. Elsayed, N.R.M. Roberts, B. Joseph, J.N. Kuhn, Low temperature dry reforming of methane over Pt–Ni–Mg/ceria–zirconia catalysts, Appl. Catal. B Environ. 179 (2015) 213–219.
[49] P. Kumar, Y. Sun, R.O. Idem, Nickel-based ceria, zirconia, and ceria–zirconia catalytic systems for low-temperature carbon dioxide reforming of methane, Energy, Fuel 21 (2007) 3113–3123.
[50] M.S. Lanre, A.E. Abasaeed, A.H. Fakeeha, A.A. Ibrahim, A.A. Alquraini, S. B. AlReshaidan, A.S. Al-Fatesh, Modification of CeNi0. 9Zr0. 1O3 perovskite catalyst by partially substituting yttrium with zirconia in dry reforming of methane, Materials, 15(10) (2022) 3564.
[51] M.S. Lanre, A.E. Abasaeed, A.H. Fakeeha, A.A. Ibrahim, A.S. Al-Awadi, A.B. Jumah, F.S. Al-Mubaddel, A.S. Al-Fatesh, Lanthanum–cerium-modified nickel catalysts for dry reforming of methane, Catalysts 12 (7) (2022) 715.